Analysis and Characterization of Yarn Parameters – a synthesis and future perspectives

Lesson Summary

Vítor Hugo Mendes da Costa Carvalho

This document is being submitted to the University of Algarve as part of the public proofs of the habilitation process, as outlined in Decree-Law No. 239/2007 of June 19, 2007.

January 2023

Faculty of Sciences and Technology

University of Algarve

This page was intentionally left blank

Summary

This document is being submitted to fulfil a requirement for habilitation public proofs, as outlined in Decree-Law No. 239/2007 of 19 June 2007. These proofs include a seminar or lesson on a topic related to the candidate's field of knowledge or specialty, along with a discussion of the topic.

The author, who is a member of the Intelligent Control and Systems disciplinary group at the Department of Technologies in the School of Technology at the Polytechnic Institute of Cávado and Ave (IPCA) and of the research centre on Applied Artificial Intelligence at IPCA, has chosen the theme of "Analysis and Characterization of Yarn Parameters – a synthesis and future perspectives" for his lesson.

Since 2002, the author has conducted and coordinated research focused on developing methodologies to automatically characterize yarn parameters to improve efficiency and quality in yarn production. This work has been funded by the Portuguese Science Foundation for Technology (FCT) and has been the subject of doctoral and master's theses, as well as final internships for bachelor's students under the author's supervision. The results of this research have been published at national and international conferences and in journals. The author's experience and involvement in this field made the selection of the lesson topic a natural choice.

The lesson covers approaches and methodologies for analysing and characterizing yarn that have been developed or co-developed by the author, as well as those that are still in development, also presenting some future ideas of further steps. It is divided into four chapters: an introduction to the topic (Chapter 1), a review of theoretical concepts (Chapter 2), a description of methodologies for analysing and characterizing yarn mass parameters (Chapter 3), and proposals for future challenges in the field (Chapter 4).

This page was intentionally left blank

Index

Acknowledgments

Over the past 21 years of the author's research in this area (15 years after earning his PhD), he has have received valuable contributions from several people and institutions, including mentors, colleagues, students, and partners. The author expresses his heartfelt thanks to mentors João Monteiro, Filomena Soares, Rosa Vasconcelos, and Michael Belsley. Furthermore, the author thanks to Paulo Cardoso, José Gabriel Pinto, Dimitri Isakov, Elsa Ribeiro, Joaquim Jorge, and José Carvalho for their assistance and cooperation. The author is also grateful to his PhD, Master, and Bachelor students, including Filipe Pereira, Nuno Gonçalves, Ricardo Pinto, Nélson Cunha (R.I.P.), Márcio Neves, Vítor Silva, Carlos Alves, Jorge Silva, and Ricardo Fernandes. The Portuguese Science Foundation for Technology (FCT) is recognized for its financial support. Finally, the author expresses his wholehearted thanks to his family, especially his wife Soraia Silva and his parents José and Maria Carvalho.

This page was intentionally left blank

1 Introduction

This chapter provides the background and motivation for the lesson topic, as well as a description of the main characteristics and constraints of commercial yarn analysis equipment for determining yarn hairiness, diameter, mass, periodic errors, and production characteristics. It also discusses recent studies on using image processing and artificial intelligence for yarn characterization.

1.1 Background and Motivation

The accurate evaluation of yarns is crucial for the textile industry because the quality of the final fabric depends on the quality of the yarn. To test yarns, various companies have developed specialized equipment, such as the Testers from Uster (in their 6th version) [1] and the Multitester from Zweigle [2] (which was acquired by Uster in 2009 and became Uster Zweigle products [3]). This equipment is known for their contributions to quantitative yarn characterization, but they are expensive, require a large installation space, and have limited resolution and precision in evaluating certain yarn parameters. As a result, some yarn producers do not have their own yarn testers and instead outsource evaluations to testing laboratories, which can be time-consuming and reduce efficiency [4].

Over the past few decades, various technologies have been used to evaluate yarn, including capacitive sensors, optical sensors, and more recently image processing and artificial intelligence [5]–[12]. The author's motivation for these studies stems from the identified drawbacks and opportunities in the available commercial equipment, which are described next.

1.2 Commercial Equipment Overview

The following sections discuss equipment used to determine yarn parameters such as yarn hairiness (as shown in Figure 1), yarn diameter variation, yarn mass variation, yarn periodic errors, and yarn production characteristics.

1.2.1 Yarn Hairiness Analysis Systems

This section describes the history of methods used to measure yarn hairiness, which refers to the number of fibres that have loosened from the yarn core (as shown in Figure 1). Traditional methods for measuring yarn hairiness include microscopy, weighing, and photoelectric methods, while image processing and artificial intelligence methods are still being developed [5]–[12].

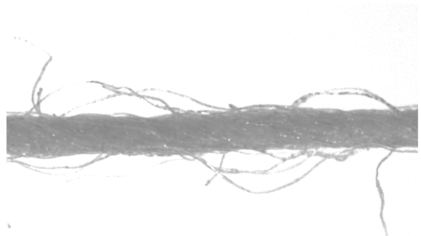

Figure 1 - Yarn image showing hairiness

Microscopic methods for measuring yarn hairiness involve examining the yarn under a microscope and counting the number of protruding hairs, loops, and their lengths in a specific section of the yarn. However, it can be difficult to accurately identify the boundaries of the yarn due to interference from looped fibres, protruding fibres, low-twisted sections, and diameter variations. This method also requires a significant number of samples, which can be time-consuming [13].

Weighing techniques involve comparing the mass of the yarn before and after singeing (burning off the protruding hairs), but this method is not precise, requires also a substantial number of samples and may not fully remove the hairiness from the yarn, especially for shorter lengths [14]. To address these issues, some equipment uses photoelectric methods. The Shirley (Atlas Hairiness Tester) uses a LED beam and photocell pair (measuring head adjustable between 1mm and 10mm) to count the number of interruptions caused by protruding hairs in the light beam. The Zweigle (G 566 Hairiness Tester) also uses this method but defines nine length zones between 1mm to 12mm or 15mm, using different optical channels [15]. This method involves using a light source and detector on opposite sides, displaced a certain distance from the yarn being analysed. When yarn hairs appear, the light from the emitter is partially blocked, indicating the presence of hairiness. This low-cost process, which uses a simple LED as a source and a photodiode or photocell as a detector, can be extended to various distances, allowing for the determination of hair lengths. Photocells can have difficulty accurately characterizing hair length due to the variety of geometric shapes that hairs can have. This method is also prone to high levels of imprecision and uncertainty. Equipment that uses red light wavelengths has improved upon previous methods, but equipment that uses crossed optical polarizers to extract the yarn core may remove important signal components for yarn hairiness characterization because the orientation of the hairiness can alter the polarization of scattered light [16]. Additionally, the contours of the yarn may be incorrectly identified as a signal due to hairs. Equipment developed by Barella, which uses a specific width mask to extract the yarn core, is also not precise as yarn alignment and traction can cause position fluctuations and diameter variations [17]. The Uster Tester 6 which is currently available on the market, continues to use photoelectric methods [1].

1.2.2 Yarn Diameter Variation Analysis Systems

To measure diameter variations, commercial systems typically use optical methods. The most well-known systems are the diameter module of Uster Testers [1] and the Oasys from Zweigle [2]. These systems use red/green light sources that transmit a certain amount of light that is blocked by the yarn. The signal received by an optical sensor (the light that is not blocked by the yarn) is proportional to the yarn diameter. In addition to these systems, Keisokki - Laserspot determines the yarn diameter using a laser and line array, based on the diffracted light that is not received by the hairiness sensor described earlier [18]. The yarn diameter is measured by the width between the edge of the first and last segment. Lawson- Hemphill also uses an optical system (EIB) with a line scan camera, where the diameter is the distance between pixels near a user-set threshold level [18]. In the Oasys - Zweigle system, the reference diameter is obtained from the first 100m of yarn, and the calibration is performed with the signal from yarn-free conditions. The Keisokki - Laserspot system is based on yarn light diffraction. The measuring field in the Oasys - Zweigle is 2mm, while the fields in the Uster Testers, Keisokki - Laserspot, and Lawson-Hemphill EIB are less than 1mm [1], [18].

1.2.3 Yarn Mass Variation Measurement Systems

Commercial equipment from Uster (Testers) [1], Zweigle (ZT 5) [2], and Keisokki (KET-80) [18] all use parallel plate capacitive sensors to measure yarn mass variation, with sample lengths of at least 5mm. These sensors work by measuring the change in capacity due to the dielectric alteration between the sensor plates caused by variations in the yarn mass sample. This allows for the establishment of a direct relationship between capacity and yarn mass [19]. However, these sensors are sensitive to temperature and humidity, which can cause unwanted fluctuations in the data. Figure 2 shows the capacitive sensors used in the yarn mass variation module of the Uster Tester 6.

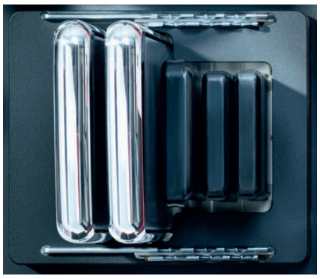

Figure *2* - Capacitive sensors in Uster Tester 6 [1]

1.2.4 Signal Processing Approaches for Yarn Periodical Errors Determination

The commercial solutions currently available for measuring hairiness, diameter, and mass variations only use Fast Fourier Transform (FFT) based signal processing techniques to detect periodic errors (as shown in Figure 3), which might not detect certain important errors.

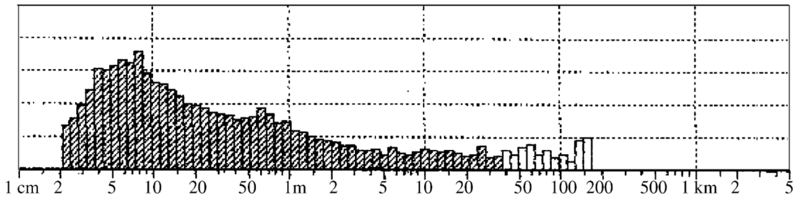

Figure 3 - Example of a spectrogram for 8mm samples with Uster Tester 3 [19]

1.2.5 Yarn Production Characteristics

There is currently no commercial equipment that can automatically determine yarn production characteristics. These parameters must be obtained manually, using methods such as microscopy or visual inspection.

1.3 Studies on the Yarn Parameters Measurement Using Image Processing and Artificial Intelligence

In addition to the yarn analysis techniques used in commercial equipment, the use of image processing and artificial intelligence to analyse yarn parameters has gained attention in yarn analysis research [11], [20]–[25]. Some recent studies in this area include Zhisong Li et al. (2020) [11], in which a system was used to assess yarn quality by obtaining parameters such as yarn diameter, faults, and hairiness using computer vision and image processing techniques. In this prototype (shown in Figure 4), the diameter image processing unit (DIPU) and a series of sampling points selected from the moving yarn are first defined. The DIPU corresponding to each sampling point is then segmented from the captured yarn images, and the average DIPU diameter is used to represent the yarn diameter at the test points. When extracting yarn images, the DIPU is divided into a foreground region, a defined background region, and an unknown region based on gray level projection distribution characteristics.

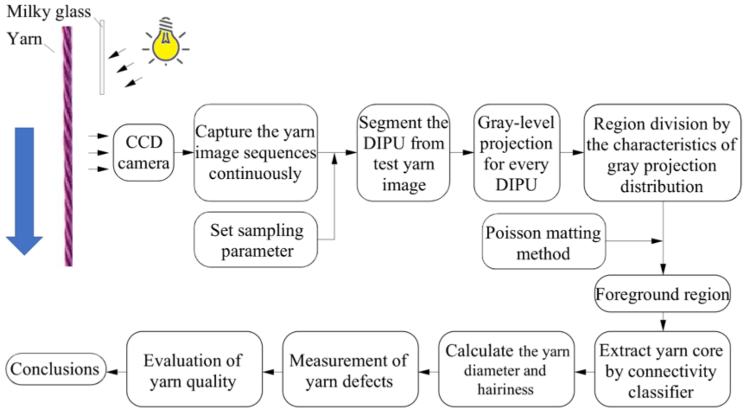

Figure 4 - Flowchart of the method for detecting yarn parameters and evaluating yarn quality (Adapted from [11]*).*

The unknown region is then further processed using the Poisson Matting method [26], which separates the yarn image and the background image completely using a defined connectivity classifier. Once the yarn core has been extracted using the classifier, hairiness is determined using image subtraction. Finally, statistical methods are used to analyse yarn faults to further assess yarn quality. Yarn hairiness has a direct impact on yarn properties, weaving efficiency, and fabric appearance. Using the method described above, the DIPU is extracted from the yarn core based on the connectivity of pixels in each image. The hairiness pixels can then be obtained using image subtraction. Figure 5 shows hairiness removal using the image subtraction method [11].

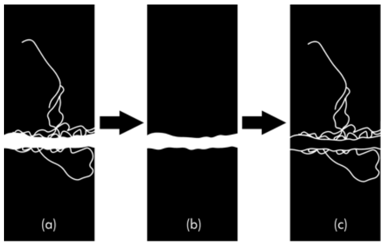

Figure 5 - (a) New foreground image, (b) yarn core, (c) hairiness (Adapted from [11]*).*

In the designed system, a closed room is used as an image capture platform to protect against stray light disturbance. A white diffused glass is used to eliminate reflected light and shadows. To simulate yarn movement, a driver and voltage controller are used. Figure 6 shows the integrated structure of this system. The yarn image capture system is mainly composed of the following parts:

- An imaging system, including a sensor, camera lens, and light source. The CCD image sensor is used to collect a sequence of images from the yarn;
- An imaging lens with a large depth of field to ensure that hairiness at different positions can be clearly analysed.

Images were acquired in the closed room using a SONY Zoom lens C with a focal length of 12.5 to 75mm, connected to a digital charge-coupled device (CCD) camera (Basler acA2040-180 km/kc, pixel size 5.5µm, resolution of 2048 × 2048 pixels, sampling rate of 180fps) and a personal computer with an image processor. The research team [11] claim that their proposed method and corresponding detection system facilitate automation and industrialization in the online detection of yarns.

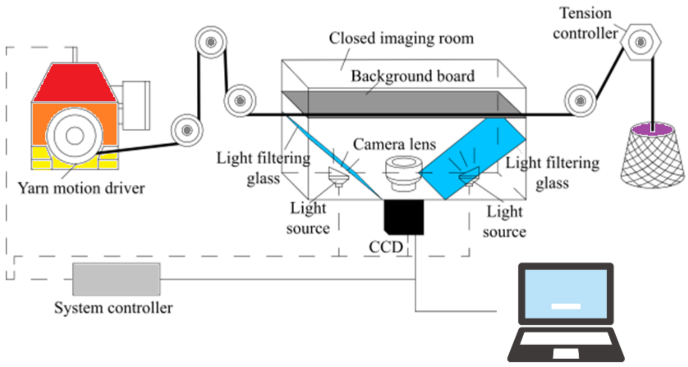

Figure 6 - System device to detect yarn parameters (Adapted from [11]*).*

Noman Haleem et al. (2021) [20] developed a system in which they argue that testing yarn in online mode can reduce latency in process control and provide fast information on yarn quality, leading to the production of high-quality yarn. They state that both capability-based uniformity test equipment and emerging image-based uniformity test systems are mostly used in offline mode and that there is currently no adequate online system that can test the quality of various yarns under normal industrial processing conditions. Therefore, they proposed an online uniformity test system for measuring a certain type of yarn fault called nep, using image processing techniques and computer vision. The developed system directly captures yarn images on a rotating frame and uses the Viola–Jones object detection algorithm [27] for real-time detection of nep faults. The authors demonstrated that the nep detection algorithms and the new method have reasonable faults detection accuracy and promising potential for use in the yarn spinning industry, through comparison with Uster's existing commercial uniformity testing equipment (Tester). Image collection was performed using a Basler 1440–220µm digital camera (Basler, Germany) equipped with a 50mm lens. The authors used three nep detection models (named A, B, and C), which are essentially image classifiers that vary in terms of the input data used in their training phase. The training data consists of positive and negative images in a 2:1 ratio, which were resized by factors of 0.2 and 0.1, respectively, to optimize training time. The number of training cycles for each model was 10. Figure 7 shows three concatenated images of yarns with the nep faults, acquired using the proposed image acquisition configuration during the yarn spinning process. The authors also found that, in an analysis of a series of images of the continuous shape of yarn, the size of the field of view was important to accommodate the lateral oscillations of the yarn during the spinning process [20].

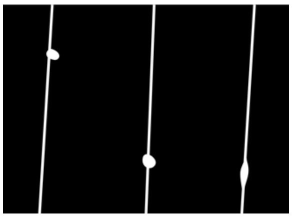

Figure 7 - Yarn image with nep faults obtained using the image acquisition system (Adapted from [20]*).*

In their work on using artificial intelligence to model yarn tensile properties, Adel El-Geiheini et al. (2020) [21] argued that the use of artificial intelligence technologies could lead to more objective yarn testing systems with specifications of higher quality products that meet the demands of manufacturers and end users. They developed a method using image processing and artificial neural networks to model the tenacity and percentage of elongation of yarns for different types of yarns. Feed-forward neural networks trained with the back propagation rule were used. Two systems were developed: the first was used to evaluate the percentage of elongation and tenacity of cotton threads, and the second was used to evaluate the parameters of mixed threads. By applying image enhancement combined with a multilayer neural network, they obtained good results in estimating different yarn parameters. Images of samples were collected with a digital camera and processed using Matlab 2015 software. Filtering and scaling were applied, and two adjustments were made to the artificial neural networks trained with the Levenberg-Marquardt back propagation algorithm [28]. The networks were trained using 80% of the dataset, while the remaining 20% was used for validation and testing. For the first model, which was the cotton yarn model, the images were enhanced by applying Gaussian filtering, then converted to grayscale and scaled to 250 x 250 pixels. The target data were then encoded and used as input vectors for the neural network. A total of 152 samples were introduced to train and validate a feed-forward back propagation neural network, which consisted of an input layer, a hidden layer with 15 neurons, and an output layer with two outputs: the tenacity (RKM) and the percentage elongation at break of the cotton threads. The second model was used to understand the tensile properties of mixed yarns. Like the first model, the images were enhanced using the Gaussian filter, then converted to grayscale and resized to 250 x 250 pixels. The target data were also encoded. A four-layer feed-forward artificial neural network was developed, with 20 and 10 neurons in the two hidden layers, respectively. Figure 8 and Figure 9 illustrate the implemented neural networks by Adel El-Geiheini et al. (2020) [21] for the first and second models, respectively. According to the authors, the use of image processing and neural networks can effectively evaluate various properties of textile yarn.

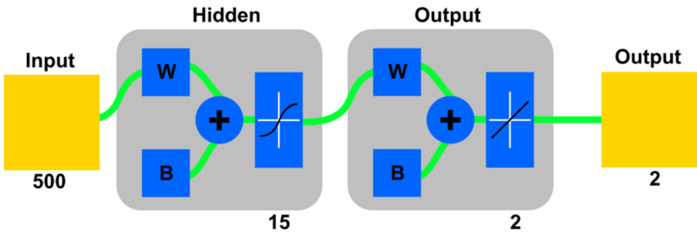

Figure 8 - Cotton threads: the architecture of neural network tensile properties (Adapted from [21]*).*

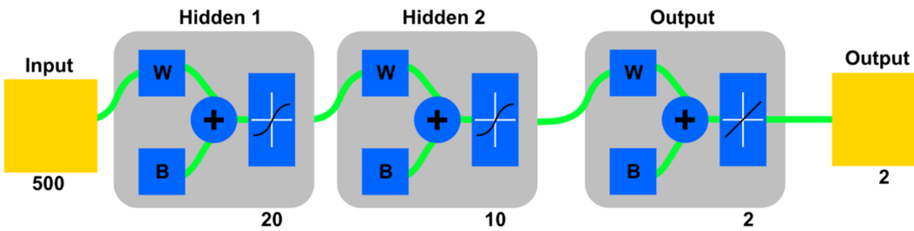

Figure 9 - Mixed yarns: the structure of neural network tensile properties (Adapted from[21]*)..*

Manal R. Abd-Elhamied et al. (2022) [22] conducted a study using artificial neural networks (ANNs) and image processing to predict the characteristics of cotton thread. The yarn characteristics were measured using Uster Tester 3, Uster Tester 5, and Uster Tensorapid4 machines. The research focused on evaluating yarn tenacity, percentage elongation, coefficient of mass variation, and percentage of yarn imperfections for spun and compact cotton yarns. Figure 10 illustrates the steps used to analyse the acquired images and input the data into the neural network.

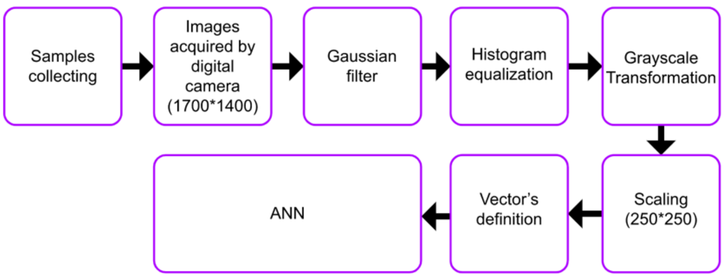

Figure 10 - Stages of the process performed (Adapted from [22]*).*

For the neural network used to assess tenacity and percentage of elongation for the ring-spun yarn system (Figure 11a), the authors designed a network with an input layer, a hidden layer with 15 neurons, and an output layer. For the second system (Figure 11b), they used two hidden layers with 20 and 10 neurons, respectively. For the coefficient of variation of yarn mass (CVm%), the same network structure was used for both systems, with 20 neurons in the first hidden layer and 8 neurons in the second layer. For the thin places, thick places, and neps of the yarn, two different network structures were used for each system. The ring yarn system had two hidden layers with 20 and 8 neurons, while the compact system had only one layer with 12 neurons, as shown in Figure 11. The authors concluded that it is possible to successfully model yarn parameters using these techniques.

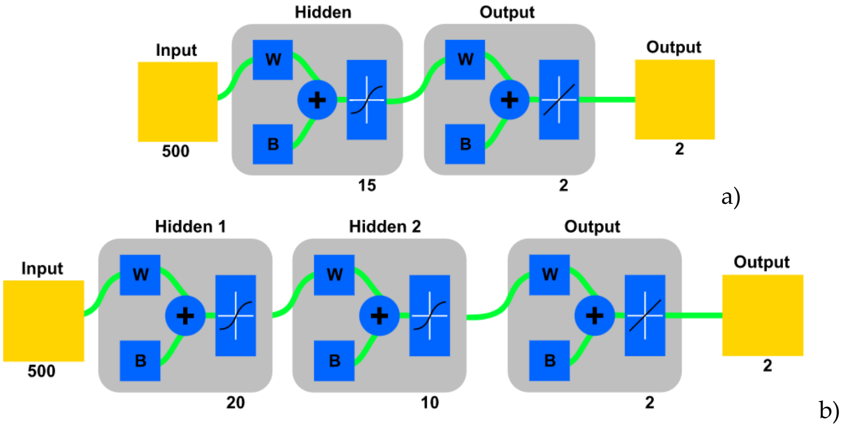

Figure 11 - The tenacity and % elongation architectures of the neural network: (a) Ring-spun yarn system (left), (b) compact yarn system (right) (Adapted from [22]).

Based on the analysis of commercial equipment and ongoing studies, there are still some gaps and opportunities where the author's research has contributed and still contributes to the yarn characterization and analysis field, including the development of a low-cost system capable of identifying and characterizing yarn parameters such as mass, hairiness, defects, and production characteristics to assess yarn quality with a superior yarn parameterization in comparison with the commercial equipment.

2 Theoretical Concepts

This chapter provides a comprehensive overview of the concepts related to yarn characterization, including textile yarn fundamentals, yarn statistical parameters, and the use of signal processing to identify yarn periodic errors and optical signal processing to obtain yarn parameters.

2.1 Yarn Characterization Parameters

This section covers the yarn parameters such as linear mass, diameter, specific volume, hairiness, twist orientation, and step and faults [29].

2.1.1 Yarn Linear Mass and Diameter

The relationship between the diameter of a yarn and its linear mass is an important aspect of yarn analysis, as it simplifies characterization. If the yarn has a cylindrical shape, the diameter is proportional to the square root of its linear mass [30]. Figure 12 shows the correlation between these two parameters in a yarn configuration.

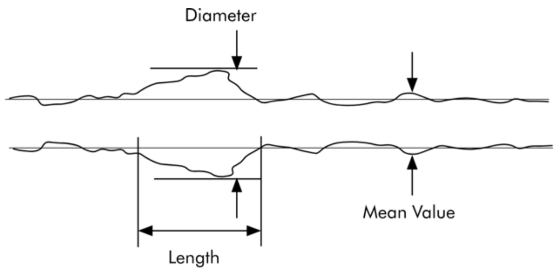

Figure 12 - Yarn configuration (Adapted from [30]*).*

The linear mass can be expressed in tex (g/km), and it is determined by equation (1) [7], [30]:

$$tex\left(\frac{g}{km}\right) = \phi \times \rho \left(\frac{g}{cm^3}\right) \times \pi \left(\frac{d\ (cm)}{2}\right)^2 \times \left(\frac{10^5 cm}{km}\right) \qquad (1)$$

$$\leftrightarrow d(cm) = \sqrt{4 \times tex/(\pi \times 10^5 \times \phi \times \rho)}$$

where: d is the wire diameter (cm); tex is the linear mass of the yarn (g/km); φ is the porosity; ρ is the density of the yarn material (expressed in g/km^3).

2.1.2 Yarn Specific Volume

The specific volume of the yarn reflects the way the fibres are packed together and is determined by the volume of the fibres and the space between them. This parameter can be calculated using its relationship with the linear mass of the yarn, as shown in equation (2) [29]:

$$V_t = \frac{\pi R^2}{N\ 10^{-5}} \qquad (2)$$

where: R is the yarn radius (mm); N is the linear mass of the yarn (g/km); V_t is the specific volume (cm^3/gm).

2.1.3 Yarn Hairiness

Hairiness refers to fibres that protrude from the body of the yarn, forming loops and emerging from the core of the yarn. It is a property that affects the appearance, feel, and use of the textile and is crucial for the final quality of the fabrics. Detecting and measuring this parameter is complex and generally requires the evaluation of multiple indicators. It is commonly measured by the length of fibres that extend out of the yarn core per unit length. In addition, measuring hairiness allows for the quantification of several statistical parameters that are important for characterizing yarn quality and, subsequently, fabric quality, such as the coefficient of variation, average deviation of mass, hairiness index, and average deviation of hairiness. Figure 13 illustrates the representation of these protruding and looping fibres along the yarn [13], [31], [32].

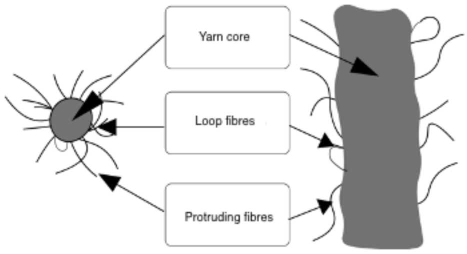

Figure 13 - Representation of the yarn core and fibres (Adapted from [32]*).*

2.1.4 Yarn Twist Orientation and Twist Step

Yarn twist orientation can be either type Z or type S. Type Z orientation is when the fibres are inclined with respect to the axis of the yarn in a way that resembles the central part of the letter Z. Type S orientation is when the fibres are inclined in a way that resembles the central part of the letter S. Figure 14 provides a visual representation of these concepts.
The twist step refers to the thickness of the fibre assembly that is being interlaced to form the core of the yarn. Figure 15 illustrates the basic concept of the twist step [33].

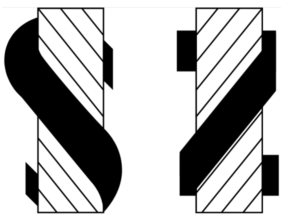

Figure 14 - Illustration of the types of yarn twist orientation[12].

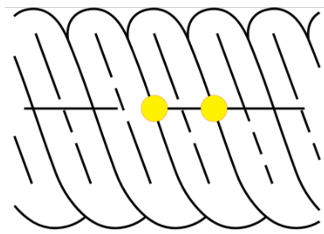

Figure 15 - Yarn twist step [12].

2.1.5 Yarn Faults

Yarn faults can be divided into three groups [33], [34]:

- Thick places: an increase in the linear mass of the yarn compared to the average value (usually less than 100% of its sensitivity). These faults are caused by a lack of force applied to the yarn during production.
- Thin places: a decrease in the linear mass of the yarn compared to the average value. These occur when waste particles appear during the manufacturing process and compress the yarn.
- Neps: a severe oscillation of the linear mass of the yarn (equal to or greater than 100% of its sensitivity) over a short distance.

Figure 16 illustrates examples of the different yarn faults.

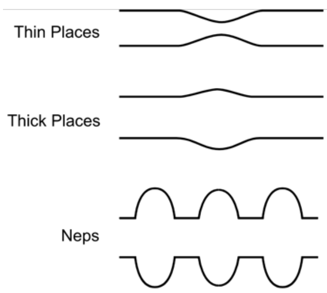

Figure 16 - Types of yarn faults (Adapted from [34]*).*

2.2 Statistical Parameters of Yarn

This section covers some important statistical parameters, including the mean deviation of mass (U%), coefficient of variation (CV%), hairiness coefficient (H), absolute deviation of the hairiness coefficient (UH%), and standard deviation of the hairiness coefficient (sH%) [35].

2.2.1 Yarn Mean Deviation of Mass

Equation (3) shows the mean deviation of mass (U%), which represents the proportionality of the variation in the mass of the samples relative to the average, regardless of the time of analysis. If the variation in mass is uniformly distributed, it tends to follow a normal distribution.

$$U\% = \frac{100}{\bar{x}T}\int_{0}^{T} |x_i - \bar{x}|\, dt \qquad (3)$$

where: x_i is the instantaneous mass; $\bar{x}$ is the average mass during the test time; T is the acquisition time.

2.2.2 Yarn Coefficient of Variation

The coefficient of variation (CV%), shown in equation (4), represents the relationship between the mean value and the standard deviation.

$$CV = \frac{100}{\bar{x}} \sqrt{\frac{1}{T} \int_0^T (x_i - \bar{x})^2 \, dt} \tag{4}$$

2.2.3 Yarn Hairiness Coefficient

Equation (5) mathematically represents the relationship of the loose ends along one meter of yarn (hairiness coefficient):

$$H = \frac{l_H}{l_{yarn}} \tag{5}$$

where: l_H is the total length of the hairiness (m); l_{yarn} is the yarn length (m).

2.2.4 Yarn Hairiness Mean Deviation

The mean deviation of the hairiness coefficient from the average is represented by equation (6):

$$UH(\%) = \frac{100}{\overline{H}N} \sum_{I=1}^{N} |H_i - H| \tag{6}$$

where: H_i is the current sample of hairiness value; $\overline{H}$is the average hairiness during analysis; N is the number of samples.

2.2.5 Yarn Hairiness Standard Deviation

Equation (7) defines the standard deviation of the hairiness coefficient.

$$sH(\%) = \sqrt{\frac{1}{N} \sum_{I=1}^{N} (H_i - \overline{H})^2} \tag{7}$$

2.3 Yarn Spectral Analysis – Fast Fourier Transform (FFT) Approach

Yarn spectral analysis involves the study of the frequency spectrum contained in a set of discrete data collected at regular intervals. It is used to identify periodic irregularities in yarn, which appear as energy spikes in the analysed frequency. To detect these spikes, a spectrogram is constructed that shows the variation of wave energy at different yarn periodicities. A Fourier transform is used to perform spectral analysis, which represents a signal in the frequency domain and reveals its frequency components. There are several Fourier transforms, but the Fast Fourier transform (FFT) is commonly used in commercial equipment and in the author's studies. This approach uses a narrowband definition to group all harmonics, as the information is highly concentrated in the spectrum. Equation (8) is used to calculate the range of energy bands per decade [36]:

$$int(I) = \sum_{I}^{I=n_{i-1}} 10^{d_i + \frac{I}{n_i}} \tag{8}$$

where: n_i is the number of intervals; d_i is the decade index (-3, -2, …, 4); I is the interval index (0, …, I).

Equation (8) uses a base 10 logarithm to obtain the coordinates of the X axis (int(I)). These coordinates evenly divide the desired number of intervals over a decade. The wavelengths detected in each energy band are summed and multiplied by the number of intervals to obtain the final value of the energy band. This process is described in equation (9):

$$e(i) = n_i \sum_{w=1}^{w=k} \lambda(w) \quad (9)$$

where: k is the number of wavelengths detected in the energy band; w is the index of the detected wavelength; λ is the wavelength in the w index.

2.4 Optical Signal Processing using Coherent Light

Consider a coherent plane wave illuminating an object and propagating through a lens towards its principal focal plane on the other side. According to Fourier optics, the electric field distribution in the focal plane of the lens is the Fourier transform of the field distribution in the object plane [13], [37]. The lower spatial frequencies of the image will be concentrated near the optical axis, while the higher spatial frequencies will be farther from the optical axis. The field distribution in the principal focal plane of the lens is given by equation (10) [38], [39]:

$$F\{g\} = \int\int_{-\infty}^{+\infty} g(x_d, y_d) e^{-j2\pi(v_{x_d} x_d + v_{y_d} y_d)} dx_d dy_d \quad (10)$$

where, $g(x_d, y_d)$ describes the field distribution in the object plane and V_{xd} and V_{yd} are the respective spatial frequencies (m^{-1}) along the horizontal (x_d) and vertical (y_d) directions, respectively.

The characteristic spatial frequency associated with an object of size d_s is given by equation (11) [37]–[39]:

$$V \approx \frac{\lambda \times f}{d_s} \quad (11)$$

where: V is the spatial frequency (m^{-1}) and f is focal distance (m) of the Fourier lens.

If there are sharp contrasts between light and dark in the object being viewed, it will produce high spatial frequencies. However, if the background illumination is relatively uniform, it will only produce low spatial frequencies. By using a small, round, opaque filter that is centred on the optical axis in the Fourier plane (as shown in Figure 17), it is possible to block the low frequency background information and allow the high frequency information about the sharp transitions between light and dark, such as the boundaries between yarn fibres or the "hairy" appearance of the yarn, to pass through (as shown in Figure 18). On the other hand, if the small, round, opaque filter is placed in the opposite position, it will eliminate the high frequencies and result in a nearly uniform background with a dark shadow of the yarn's core diameter [37], [40].

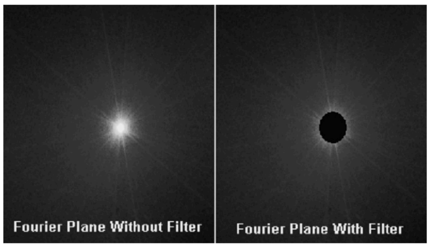

Figure 17 - High-pass spatial filter in the Fourier plane [37]

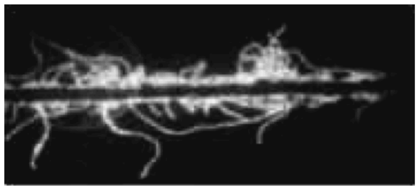

Figure 18 - Image obtained from coherent signal processing [37]

3 Methodologies of Yarn Mass Parameters Analysis and Characterization

This chapter presents the methodologies and approaches developed by the author or under the author's coordination for yarn mass parameterization using capacitive sensors, optical sensors, image processing, and artificial intelligence [8], [9], [12], [19], [30], [35], [37], [40]–[46].

3.1 Yarn Mass Parameterization using 1mm Capacitive Sensors

The purpose of this section is to describe the research conducted to create a measurement system for detecting variations in the mass over 1mm yarn using capacitive sensors [19]. A capacitive sensor with parallel plates was created and paired with an electronic conditioning circuit to accurately measure the mass of 1-4mm yarn samples. The research found that a 57tex (0.057g/m) yarn would produce a capacitance variation of 2.08E-17F. To improve the signal to noise ratio (SNR), a design for the conditioning circuits was implemented. To address the issue of radiation, the solution involved using two sensors in a differential configuration [19], [44] (Figure 19).

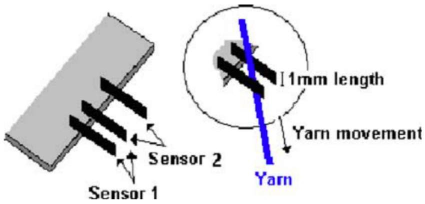

Figure 19 – Multiple plate parallel capacitive sensors [19]

The differential configuration helps the electric circuit maintain stability in the face of temperature and humidity fluctuations, which are common in the textile industry. The experimental setup for yarn mass measurement included a personal computer with a data acquisition system, a 1mm sensor, and the necessary electronics. The system diagram is shown in Figure 20.

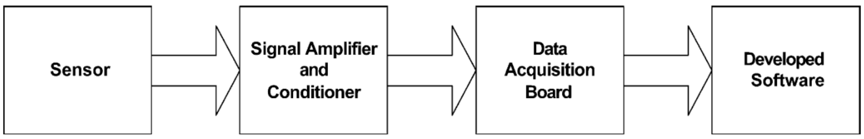

Figure 20 – Yarn mass measurement system flowchart [19]

To create two capacitors with a shared electrode, the system design included three metallic conductors placed in parallel. The integrated circuit (IC) MS3110 from Microsensors was utilized for amplifying the transducer and conditioning the signal. It is specifically designed for use with capacitive sensors and has a capacitance resolution of up to 4.0aF/rtHz, a programmable bandwidth adjustment between 0.5-8kHz, and on-chip EEPROM for storing settings [44]. The sensor's capacitance variation is converted into a voltage signal, amplified, and then filtered through a second-order low-pass filter to eliminate high-frequency interferences from the internal oscillator and external noise sources. The filtered signal is then amplified again (Figure 21).

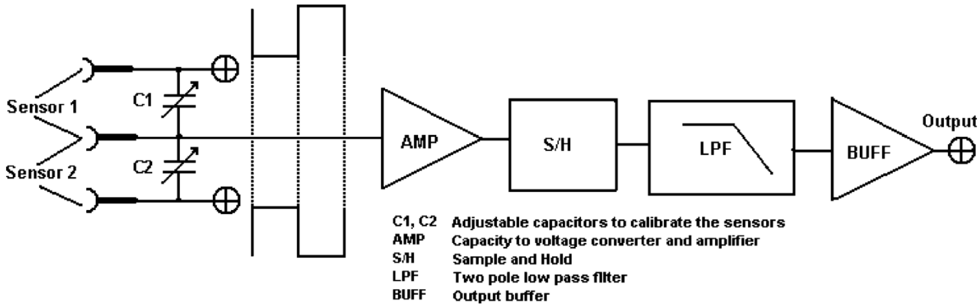

Figure 21 – Dual sensor parallel plates and MS3110 IC block diagram [19]

The output signal is converted into digital form using an ADC (analogue to digital converter) found on the data acquisition board (6024E from National Instruments). The data is monitored on a personal computer using control software developed with LabVIEW®. This software allows the storage, manipulation, and processing of data for analysis of the results obtained.

3.2 Yarn Hairiness and Diameter Parameterization using Optical Sensors and Image Processing

The research described in this section focused on using coherent signal processing techniques to create modules for measuring yarn hairiness and diameter [35], [37], [40], [45].

3.2.1 Yarn Hairiness Parameterization using Optical Sensors

This sub-section describes the approach developed for measuring yarn hairiness [35], [37], [45].

3.2.1.1 Yarn Hairiness Optical and Electronic System Design

The hardware for measuring yarn hairiness consists of two main modules: the electronic module and the optical module. The electronic module includes a photodiode (S1227-1010BR) from Hamamatsu® as the receiver. Some of its key features include a measurement area of 10mmx10mm, sensitivity to the He-Ne Laser emitting at a wavelength of 632.8nm of 0.39A/W, a maximum dark current of 50pA, a shunt resistance of 2GOhm, and a terminal capacitance of 3000pF. A conditioning circuit was designed featuring a high-precision current to voltage converter based on a Burr-Brown operational amplifier OP277P (Figure 22) [47].

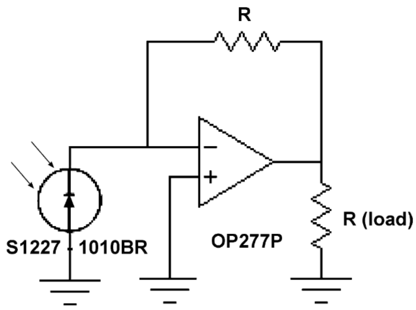

Figure 22 - Current to voltage converter [37]

Since the operational amplifier offset and photodiode dark current are significantly smaller than the signal magnitude, they can be ignored. As long as neither the photodiode nor the operational amplifier becomes saturated, it can be established a direct proportional relationship between the photodiode current and the output voltage using equation (12).

$$V_{R_{\text{load}}} = -RI_{\text{photodiode}} \tag{12}$$

The output of the operational amplifier is connected to an analogue channel of the data acquisition board (PCI-6024E from National Instruments), and a LabVIEW® based software acquires and processes the data. Figure 23 shows the optical system developed for yarn hairiness determination.

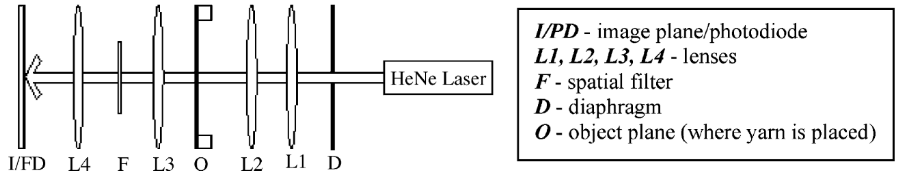

Figure 23 - Optical system design [37]

The optical setup is designed to increase the contrast of the optical signal produced by yarn hairiness. The yarn being studied is placed in the object plane. The goal of the optical setup is to generate a signal proportional to yarn hairiness in the final image plane (the position of the photodiode in Figure 23). Coherent light from a HeNe laser passes through a variable diaphragm to ensure good transverse spatial profile, then through a two-lens beam expander telescope (L1 and L2) and is directed at the yarn in the object holder. The size of the object image is controlled by lenses L3 and L4. A custom-fabricated spatial filter (F) placed in the Fourier plane of L3 processes the image by allowing only high spatial frequencies to propagate (high-pass spatial Fourier filter), resulting in the contours of the yarn and associated hairs being highlighted while simultaneously eliminating the constant background (Figure 18). To improve the SNR, a linear polarizer was placed before the object plane [38], [39]. This highlights the contours of the yarn and associated hairs while eliminating the constant background associated with the portion of the laser beam not obstructed by the sample. This method allows a higher portion of the processed optical signal to be associated with the presence of hairs on the yarn. However, there is still some signal coming from the contours of the yarn itself and light scattered by the optical elements. To characterize this "background signal," it is eliminated the yarn's hairiness by wetting it with water or quickly passing it through an open flame to burn off the "hairs." When the wet or burned yarn is placed in the object plane, it is obtained a "background signal" designated by voltage without hairiness (Vwh). Using the optical measurement setup shown in Figure 23, a significant amount of background light still reached the photodiode, likely due to the use of uncoated optical elements. This background was reduced by using a linear polarizer from Spindler & Hoyer, resulting in almost a background-free signal, and significantly increasing the dynamic range of hairiness measurements.

3.2.1.2 Yarn Hairiness Measurement Length Calibration Procedure

This study involved isolating a single hair in the yarn with a diameter of 0.64mm (Figure 24).

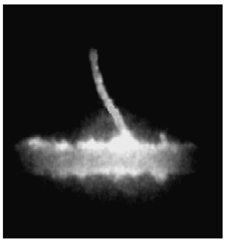

Figure 24 - Hair isolation in a 0.64mm diameter yarn [37]

To isolate the hair, silicone was used to remove all other yarn hairs. Water was not used to avoid the problem of drying, which could have caused undesired hairiness to appear over the extended test duration. The isolated hair was then stretched and oriented perpendicular to the yarn. However, to ensure that the photodiode only received a signal from the hair itself, an opaque "window" was placed in front of the photodiode to block the signal from the yarn's borders, which were somewhat enhanced due to light scattering from the silicone, which has a high refractive index. The "window" had an adjustable aperture to allow measurement of the output voltage as a function of hair length. The hair had an actual length of 2.67mm, but after being imaged by the lenses, the projection of the hair on the photodiode had a length of 1.50mm, meaning that the actual hair length was reduced by 44% due to the optical elements needed to image the signal on the photodiode. The measurement process involved reducing the aperture in steps of 250µm and taking seven separate readings, starting with the window fully opened and gradually closing it. The hair was then removed, and the window was gradually opened to record the background signal at each aperture setting, which was subtracted from the corresponding values obtained with the hair. The operational amplifier offset signal (value measured with no light signal) was also subtracted from all measurements. A linear correlation was obtained for the final curve (output-noise-offset) (Figure 25).

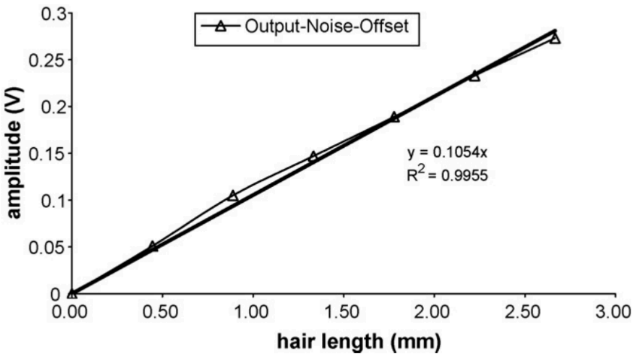

Figure 25 - Hairiness length calibration curve [37]

In this case, the output signal (y) is related to the hair length (x) by the expression y = 0.1054x, which means that for every millimetre of hair length, the output increases by 105.4mV for the gain used in these tests.

3.2.1.3 Yarn Hairiness Minimum Statistical Reference Method

This method is based on the fact that, even for extremely hairy yarns, a significant number of observations made in 1mm samples of yarn will correspond to sections without hairiness. Figure 26 shows an electron microscope image that supports this claim for a particular yarn with high hairiness. It is possible to see that there is a 1mm region where no hairiness is observed.

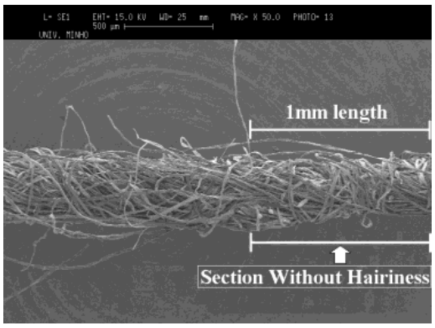

Figure 26 - Image of a yarn with a region of 1mm without hairiness [45]

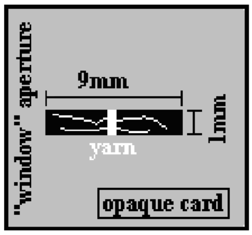

Figure 27 - "Mask" used [45]

A mask was created using an opaque card with a 9mmx1mm aperture to measure yarn samples of 1mm length with the 9x10mm^2 photodiode. This mask was placed in front of the photodiode, allowing measurements to be taken in 1mm increments (Figure 27). An acquisition software module using LabVIEW® was also developed for this purpose.

After developing the acquisition system, an algorithm for implementing the statistical reference method was designed and implemented using LabVIEW®. Its steps are:

1. Determine the minimum value, average value, and standard deviation of all samples.
2. Determine the number of 1% increases, step by step, needed to reach the average value (M) starting from the minimum value.
3. For each increase up to the average, determine the number of samples and their values in the interval [minimum; increased value].
4. Determine the average value of the elements in each tested interval and their corresponding standard deviation.
5. Calculate the median of the average values obtained in step 4, the step in which it is located, as well as the inferior median and superior median.
6. If the yarn is classified as: low level of hairiness (σ ≤ 0.1) - the reference is the linear interpolation between the superior median and the average; high level of hairiness (σ ≥ 0.2) – the reference is the inferior median; medium level of hairiness (σ > 0.1 and σ < 0.2) – the reference is the superior median.

This procedure was designed to produce reference values like those obtained using the water method. To do so, the interval of steps was divided at the median point into lower and upper segments. The median of the lower interval is referred to as the inferior median, while the superior median is the corresponding value of the upper segment.

A comparison between the water reference and the minimum statistical reference was performed using the same section of yarn for several yarns tested. Figure 28 presents the results obtained.

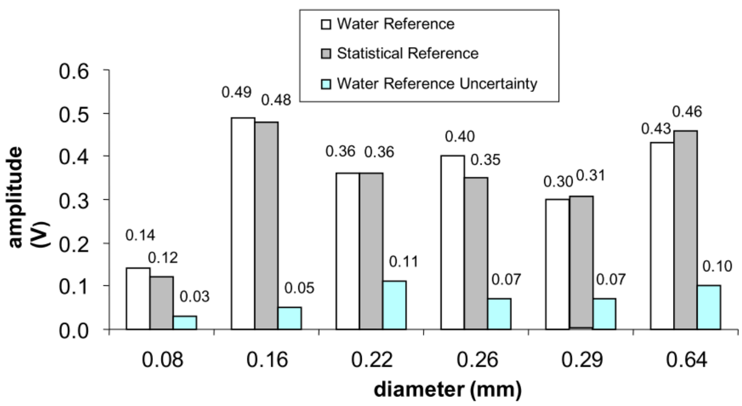

Figure 28 - Minimum statistical reference vs water reference results [45]

From Figure 28, the water references are very similar to the minimum statistical references, even for yarns with high dispersion (0.64mm). In all cases, the difference between the two methods is less than the uncertainty associated with the water method. Therefore, the method can be considered a reliable and convenient reference procedure.

3.2.2 Yarn Diameter Parameterization using Optical Sensors

In this section, the yarn diameter parameterization approach developed is described [40].

3.2.2.1 Yarn Diameter Optical and Electronic System Design

Measuring the diameter required a similar optical and electronic design as the one used for yarn hairiness parameterization described earlier. The main difference is that a low-pass optical filter was used in the setup shown in Figure 23 (Figure 29). This filter eliminated the signal from the small protruding hairs, leaving only the main shadow due to the yarn core. The low-frequency spatial image is dominated by the shadow of the yarn core superimposed on the relatively smooth background of the incident laser beam. Figure 30 shows images of yarns with different diameters resulting from the use of a low-pass spatial filter, which is the complement of the high-pass spatial filter used in the hairiness measurements. As expected, the hairiness signal is almost completely absent.

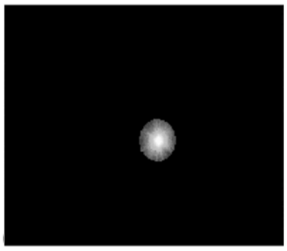

Figure 29 – Low-pass filter in the Fourier plane [40]

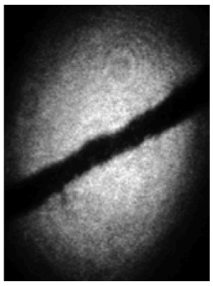

Figure 30 – Example of the application of a low-pass filter [40]

3.2.2.2 Yarn Diameter Determination Calibration Procedure

A reliable and robust method of system auto-calibration was developed to accurately determine yarn diameters and classify irregularities without the need for a conditioned atmosphere. The following steps were followed:

a) measure the signal without yarn (Vsf) (V);

b) measure the signal with yarn for various samples (Vcf)(V);

c) determine the average signal with yarn (Vcfa) (V), which represents the average diameter;

d) calculate the average signal blocked by the yarn (Vf=Vsf-Vcfa) (V);

e) use the theoretical relationship between yarn diameter and linear mass (tex=g/km), $d(mm)=4{,}44x10^{-2}\sqrt{(tex/p)}$ [30] and the sample length (sl) of the system (mm) to estimate the average area blocked by the yarn, Afsj=sl*d(mm^2);

f) determine the attenuation sensitivity for the tested yarn, Sa=Vf/Afsj (V/mm^2).

To determine the yarn diameter for each sample, the following steps were taken:

g) determine the area blocked by each yarn sample, Ai= (Vsf-Vcf)/Sa(mm^2);

h) determine the diameter for each yarn sample, di=Ai/sl(mm).

To characterize yarn irregularities, a simpler five-step process was used:

a) measure the signal without yarn (Vsf) (V);

b) measure the signal with yarn for various samples (Vcf)(V);

c) determine the average signal with yarn (Vcfa) (V);

d) determine the reference (Vr=Vsf-Vcfa) (V);

e) determine the percentage variation of each sample with yarn, di(%)= 100*(Vsf-Vcf)/Vr).

In this procedure, the signal without yarn is first measured (step a). Then, the signal with yarn is measured for various samples (step b). The average of the signal with yarn is then determined (step c). The reference (0% of diameter variation) is established by finding the difference between the signal without yarn and the average signal with yarn (step d). Finally, the percentage variation in diameter of each sample is calculated relative to the reference, using the ratio between the voltage signal blocked by the yarn sample and the reference (step e). This allows for the characterization of yarn irregularities by estimating the deviation in diameter of each sample from the reference value.

3.2.3 Yarn Hairiness and Diameter Parameterization using Image Processing

This section describes the research conducted to implement yarn characterization techniques using image processing [9]. The techniques were developed to automatically measure yarn parameters such as diameter, hairiness, and irregularities while the yarn was in a stationary state. The techniques were also used to identify and quantify loop and protruding fibres in the yarn. The methods were initially developed using image processing techniques, and later artificial intelligence techniques were applied for further improvement.

3.2.3.1 Yarn Image Acquisition System Design

The developed system for characterizing yarn using image processing consists of a low-cost analogue microscope coupled with a common web CMOS camera for image capture. The microscope provides sufficient amplification and image detail, and there were no specific requirements for the camera resolution. The flowchart for the system is shown in Figure 31.

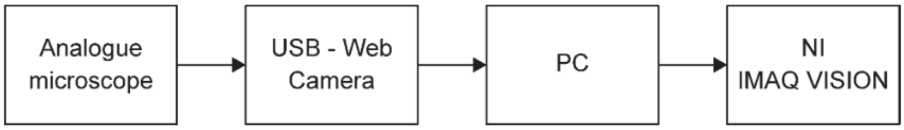

Figure 31 - Image acquisition system design [8]

The Biolux microscope from Bresser, with 5x and 16x ocular lenses and 4x, 10x, and 40x objectives, was equipped with a 2x Barlow lens and LED illumination. For this research, the 5x ocular lens was used with the 4x objective and the 2x Barlow lens, resulting in an overall magnification of 40x. This magnification was sufficient for analysing yarns with a range of linear masses. The USB web camera used was the Deluxe model from Hercules, which has a 1/4 CMOS sensor, a resolution of 640 x 480 pixels, and a colour format of 24 bits. The camera was placed at the exit plane of the microscope ocular to capture the analogue image produced by the microscope. To improve contrast for the yarn geometry, the illuminated yarn surface was kept as close as possible to a monochromatic light source. As the white LED illumination emitted a range of wavelengths, an external yellow light source was used instead. To calibrate the images, an object with known dimensions was photographed, and the distance between the lines in the image was found to be 73 pixels. This means that each pixel corresponds to 1/73mm. To analyse the images, an image processing application was developed using the IMAQ Vision software from LabVIEW®.

3.2.3.2 Yarn Diameter and Faults Parameterization using Image Processing

The process outlined in Figure 32 utilizes image processing techniques to determine the contours of the yarn core, excluding any hairiness surrounding it. The diameter is calculated by detecting edges along a series of parallel search lines and measuring the distance between the pairs of edges found by each search line. The average of these distances is taken to determine the diameter. The yarn mass can then be estimated based on the relationship between linear mass and diameter previously shown in section 2.1 [30], [46], [48].

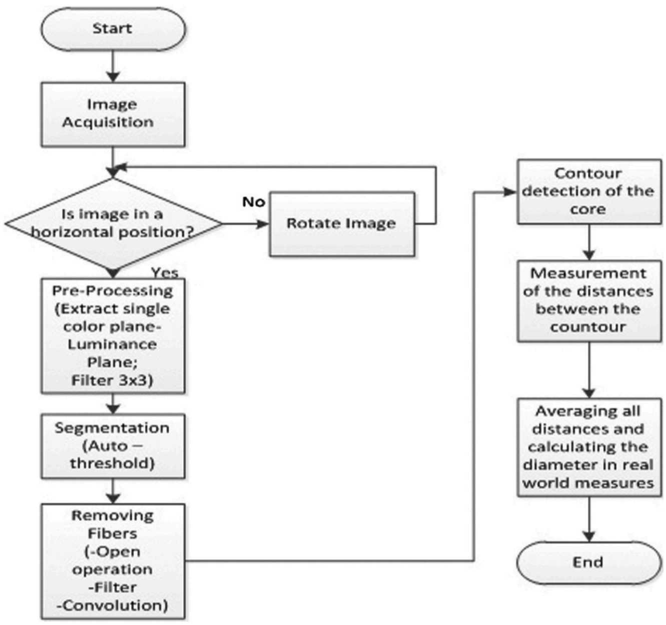

Figure 32 - Diameter determination flowchart using image processing [9]

Figure 33 to Figure 43 present an example of application of the diameter determination algorithm [9].

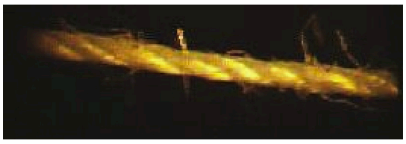

Figure 33 - Initial sample image acquisition of a 22tex yarn [9]

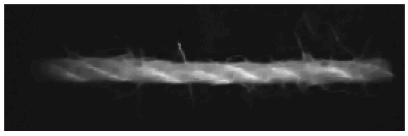

Figure 34 - Image after application of the Filter function [9]

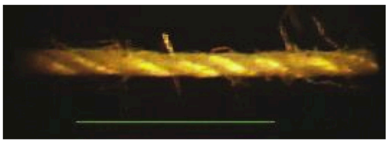

Figure 35 - Image after yarn rotation [9]

Figure 36 - Image after application of the Auto Threshold function [9]

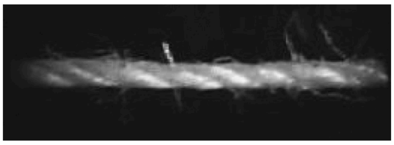

Figure 37 - Image after Removal of the Luminance Plane [9]

Figure 38 - Image after the Remove Particle function [9]

Figure 39 - Image after application of the Open function [9]

Figure 40 - Image after the application of the Canny Edge Detection function [9]

Figure 41 - Image after the application of the Convolution function [9]

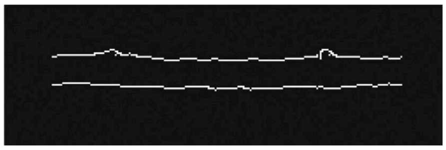

Figure 42 - Image after application of a Logical AND function using a rectangles mask [9]

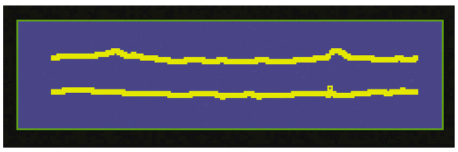

Figure 43 - Final image to determine the yarn diameter with the Clamp Vertical Max function [9]

To determine yarn irregularities, the distances between yarn fibres are measured along the yarn and compared to the average diameter (Figure 44). These measurements are collected in an array, and reference values for faults are calculated. If a measurement falls below 50% of the average diameter, it is considered a thin place. If it is above 40% of the average diameter, it is considered a thick place. If it is above 100% of the average diameter, it is considered a nep. To ensure that the fault determination is accurate, the current determination is compared to the previous one, and if they do not match, it is not considered a fault [42].

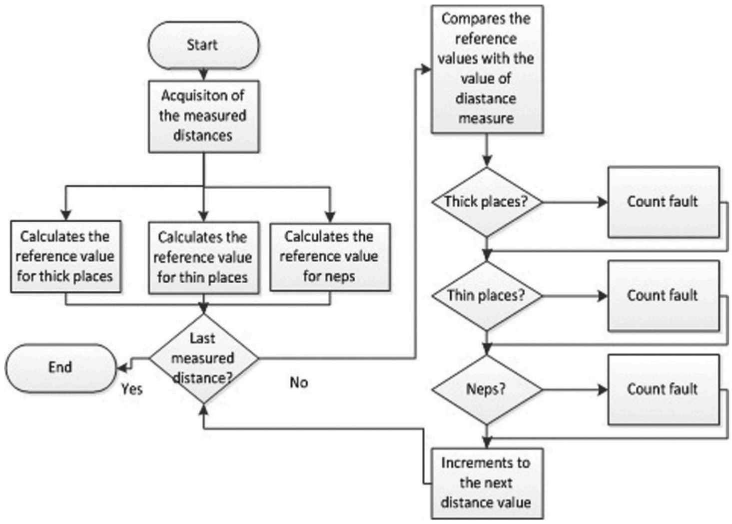

Figure *44* - Yarn faults detection flowchart [9]

3.2.3.3 *Yarn Hairiness Parameterization using Image Processing*

This study employed spatial pre-processing techniques, as well as segmentation and spatial filtering techniques, to isolate the yarn core and to identify and quantify the protruding and loop fibres from the original image. The protruding and loop fibres were isolated from the yarn using logical operators applied to the image of highlighted fibres and the yarn core. The final stage involved the removal of small objects and skeletonization of the isolated fibres to measure the hairiness coefficient. The implemented algorithm is shown in Figure 45 [42].

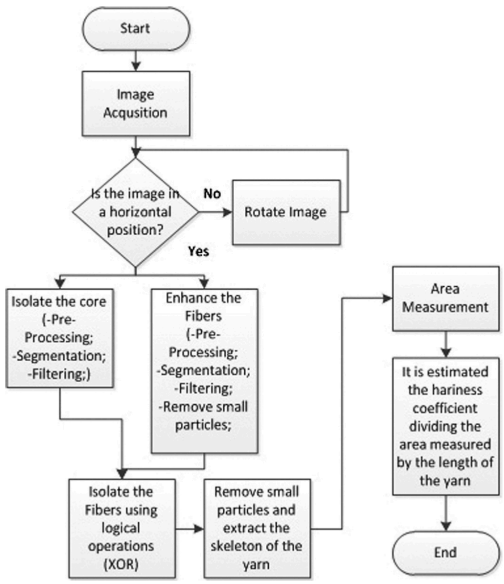

Figure *45* - Hairiness determination algorithm flowchart [9]

Figure 46 to Figure 57 present an example of application of the hairiness determination algorithm [9].

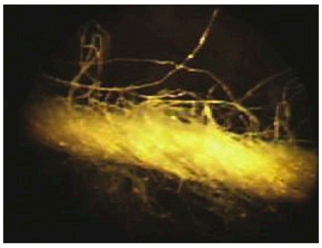

Figure 46 - Initial sample image acquisition [9]

Figure 47 - Image after the Auto Threshold function [9]

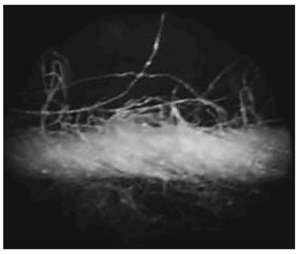

Figure 48 - Image after rotation [9]

Figure 49 - Image after the Filter and Remove Particles function [9]

Figure 50 - Image after Inverse function [9]

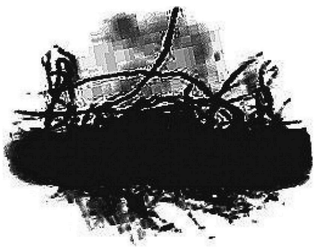

Figure 51 - Image after the Convolution function [9]

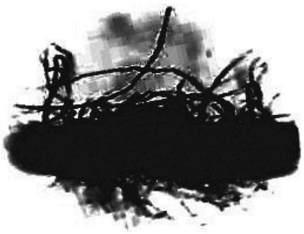

Figure 52 - Image after the Equalize function [9]

Figure 53 - Image after the Threshold and Small Particles Removal function [9]

Figure 54 - Image after the Logical Operation function and Small Objects Removal function [9]

Figure 55 - Mask to eliminate borders [9]

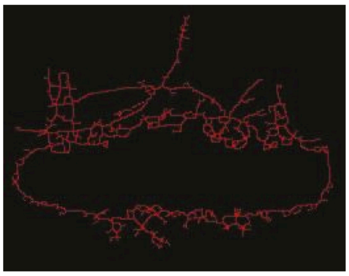

Figure 56 - Image after the Skeleton function [9]

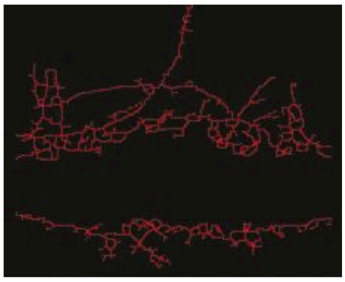

Figure 57 - Image after the Logical operation between the previous 2 images [9]

The hairiness of the yarn can be determined by using the Particle Analysis Report function on Figure 57. The width of the fibres is reduced to one pixel through skeletonization, and the measured area represents the length of the fibres in pixels. The hairiness coefficient is calculated by dividing the measured area by the length of the yarn. Moreover, and as there is currently no commercial equipment available that can detect and distinguish between loop and protruding fibres, a preliminary methodology using image processing techniques that can analyse the type of hairiness was performed. Figure 58 shows the flowchart of the applied algorithm, which begins by examining each row and column of the image vector. If a sequence of 1's pixels is found in the same row, it is considered a loop fibre. If a column with a sequence of 1's pixels is found, it is considered a protruding fibre. This initial approach only considers a sequence of 1's as a loop fibre if the current value and the next value to be analysed are both 1, and the previous value must be 0. Although further studies are needed to refine and improve the accuracy of this method for distinguishing between different types of hairiness.

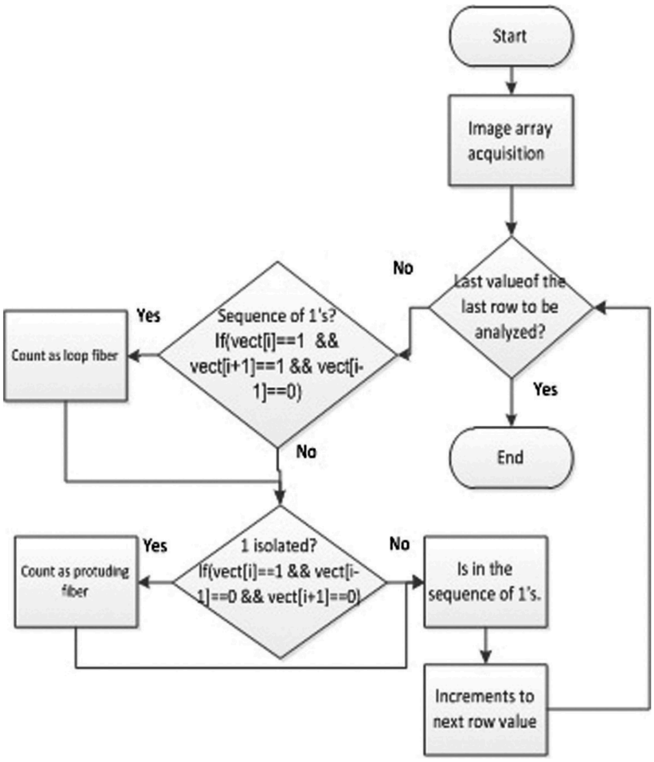

Figure *58* - Flowchart of the loop and protruding fibres distinction algorithm *[9]*

3.2.4 Yarn Hairiness Characterization using Artificial Intelligence

A methodology under development for training and classifying yarn hairiness using deep learning is described in this subsection. The first phase of this approach involved the collection of yarn images, each of which may contain multiple instances of hairiness. These images were captured using an updated vision system with proper lighting to ensure high quality. The mechatronic system shown in Figure 59 integrates the vision system and is capable of unwinding and winding the spool of yarn and consists of several components as listed in Table 1 [12].

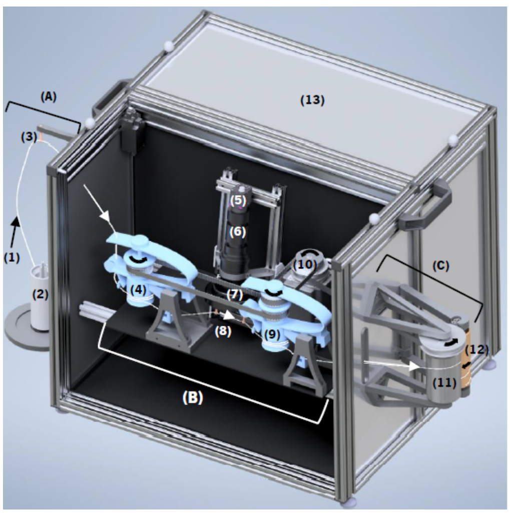

Figure 59 – Mechatronic system developed (description presented in Table 1) [49].

Table 1 – Nomenclature of mechanical system components [49].

Alphanumeric Reference	Numerical Reference
(A) Unwinding subsystem	(1) Textile yarn
(B) Conduction subsystem	(2) Coil to unwind
(C) Winding subsystem	(3) Ceramic guide
	(4) Positive feeder 1
	(5) Camera
	(6) Camera lens
	(7) Ring of light
	(8) Ceramic guides
	(9) Positive feeder 2
	(10) Servomotor
	(11) Grooved cylinder

To acquire images and videos of yarn for analysis, an OMRON model from the USB3 Vision product range was used. The specifications of the model used are listed in Table 2.

Table 2 - Camera technical specifications [12].

Model	**STC-MBS163U3V**
Interface	USB3 Vision
Sensor type	CMOS
Resolution	1.6 MP (Megapixels)
Resolution (columns x rows)	1440 × 1080 pixels
Pixel Size (L x F)	3.45µm × 3.45µm
Frame rate	238 FPS (frames per second)
Colour spectrum	Gray scale
Model	USB3 Vision
Interface	CMOS
Sensor type	1.6 MP (Megapixels)
Resolution	1440 × 1080 pixels

In addition to the camera, a set of magnifying lenses were also utilized, which can increase the magnification of the original image by 22 times.

3.2.4.1 Dataset and Annotations

An initial approach was performed using a dataset of 50 images of cotton yarn which was hosted on Roboflow [50]. These images were divided into two classes of annotations: protruding fibres and loop fibres (each image contained multiple annotations of protruding and loop fibres, resulting in a dataset of hundreds of class annotations, as shown in Figure 60). Using this dataset and the annotations made in polygonal mode with LabelME [51] several tests and training tasks were conducted to develop a model capable of identifying and classifying hairiness in real time as either loop fibres or protruding fibres.

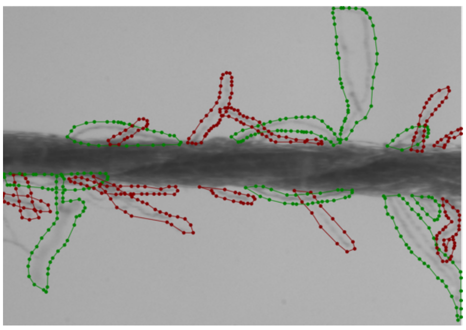

Figure 60 - Annotations of an image of the yarn made by LabelME (loop fibres—green colour and protruding fibres—red colour)[12].

3.2.4.2 Data Augmentation

Data augmentation is a set of techniques that generates new images from existing ones to artificially increase the amount of data available. Its purpose is to both quantitatively and qualitatively improve the dataset used for training, as a larger and higher quality dataset typically leads to better results. In this case, data augmentation for the training dataset was carried out using Roboflow and included adjustments to saturation (-25% to +25%), blur (up to

5px), noise (affecting up to 5% of pixels), and bounding box flipping (horizontal and vertical) (Figure 61).

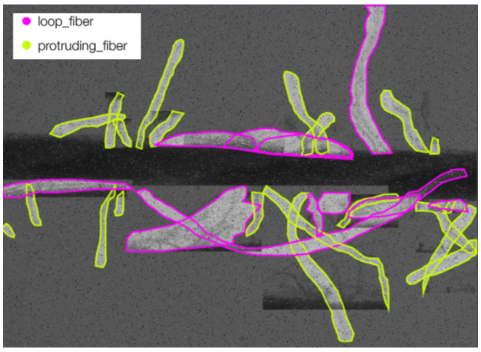

Figure 61 - Data augmentation (noise) of the dataset used in the project [12].

3.2.4.3 Algorithms, Metrics and Obtained Results

According to the confusion matrix shown in Figure 62, this initial scenario had success in classifying protruding fibres but was not able to accurately classify loop fibres.

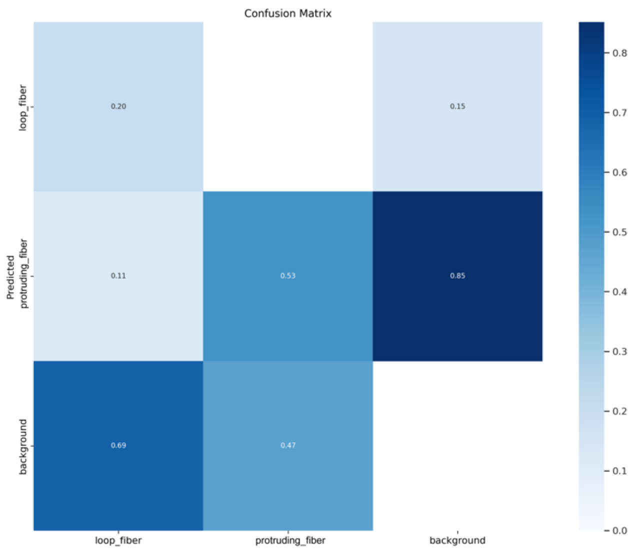

Figure 62 - Obtained confusion matrix for the training setup [12].

The output results for the YOLOv5s algorithm [52], [53] using the training dataset are shown in Figure 63. A total of 150 epochs were required to achieve a satisfactory precision, recall, and mean average precision (mAP). Further iterations did not result in a significant improvement. These metrics were calculated using equations 13 to 15 [12], [54], [55]:

$$Precision = \frac{TP}{(TP + FP)} \tag{13}$$

$$Recall = \frac{TP}{(TP + FN)} \tag{14}$$

$$IoU = \frac{Intersection\ Area}{Union\ Area} \quad (15)$$

where: TP denotes true positives, FP denotes false positives, and FN denotes false negatives. Precision reflects the accuracy of the predictions, recall measures how well all positives are detected, mAP@.5 or mAP@50 or IoU = 0.50 is the mean average precision with an Intersection over Union (IoU) threshold of 0.5 or 50%, and mAP.5:95 is the mean average precision over a range of IoU thresholds from 0.5 to 0.95.

Table 3 presents the training configuration setup and results. The calculations were performed on a laptop computer with an Intel Core™ i7-10750H CPU @ 2.60 GHz and 32 GB of RAM.

Table 3 - Training configuration/results[12].

Image Size (pixels)	1280 × 1024
Number of training images	90
Number of test images	7
Number of validation images	4
Algorithm	YOLOv5s
Epochs	150
Batch size	8
Training time (minutes)	40

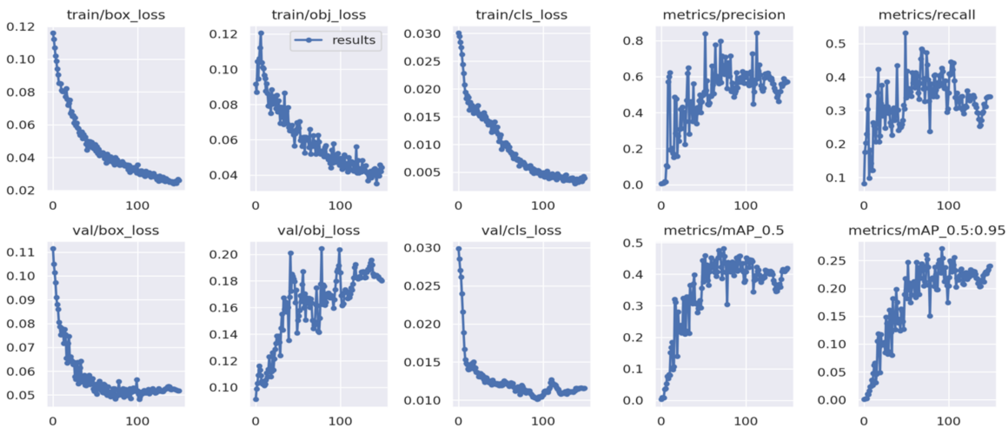

Figure 63 - Setup output results using YOLOv5s algorithm [12].

Figure 64 shows some examples of the classification results obtained during this phase of the training process. These results were used to validate and refine the classification model. Some instances of hairiness were not yet classified due to the small size of the dataset used at this stage (even though the dataset contained hundreds of class annotations, the number of possible combinations of hairiness variations may require an even larger dataset). Despite this, the results obtained at this phase with YOLOv5s were promising. Using higher versions of YOLOv5 did not significantly improve the results and came at the cost of increased computational demands.

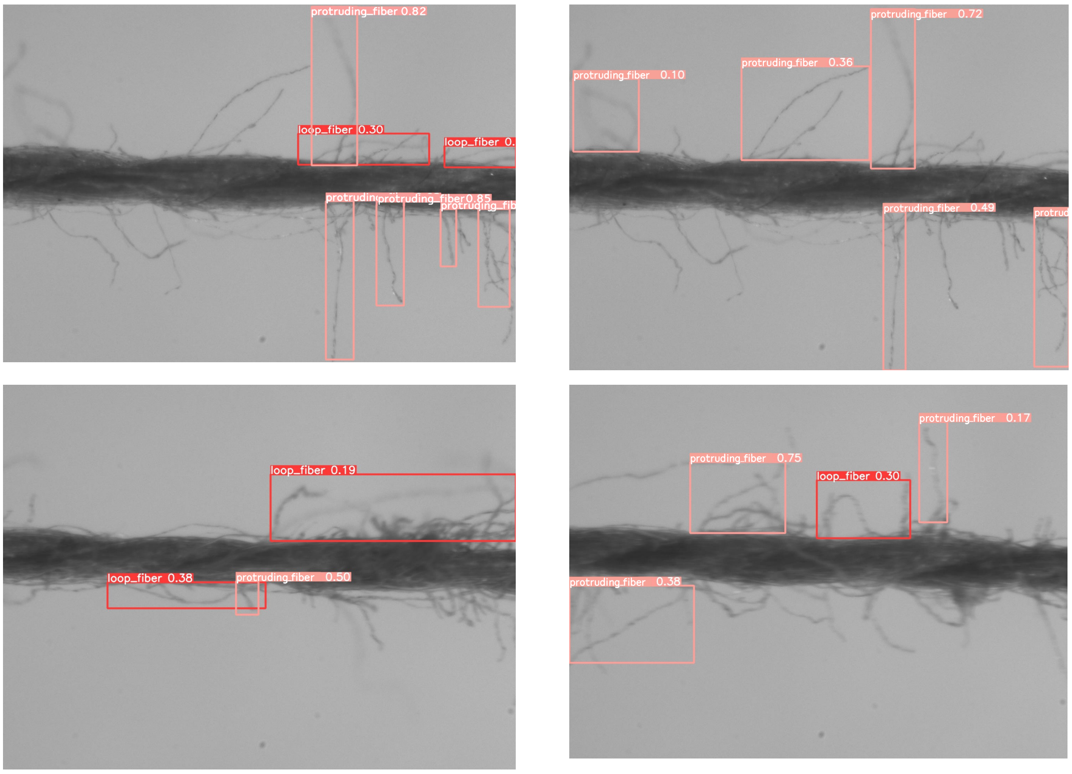

Figure 64 - Examples of classification results using the YOLOv5s algorithm [12].

A second approach was then performed increasing the dataset to 150 images. Table 4 presents the training configuration setup and results. The confusion matrix is shown in Figure 65, the output results are shown in Figure 66 and some examples of classification results are shown in Figure 67.

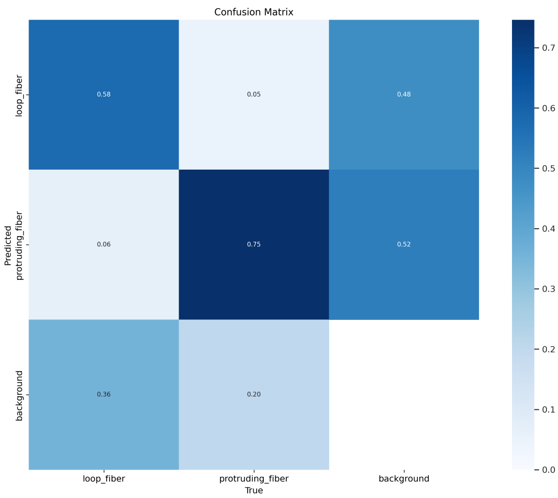

Figure 65 - Confusion matrix (dataset of 150 images)

Table 4 -Training configuration/results

Image Size (pixels)	1280 × 1024
Number of training images	315
Number of test images	30
Number of validation images	12
Algorithm	YOLOv5s
Epochs	100
Batch size	16
Training time (minutes)	39

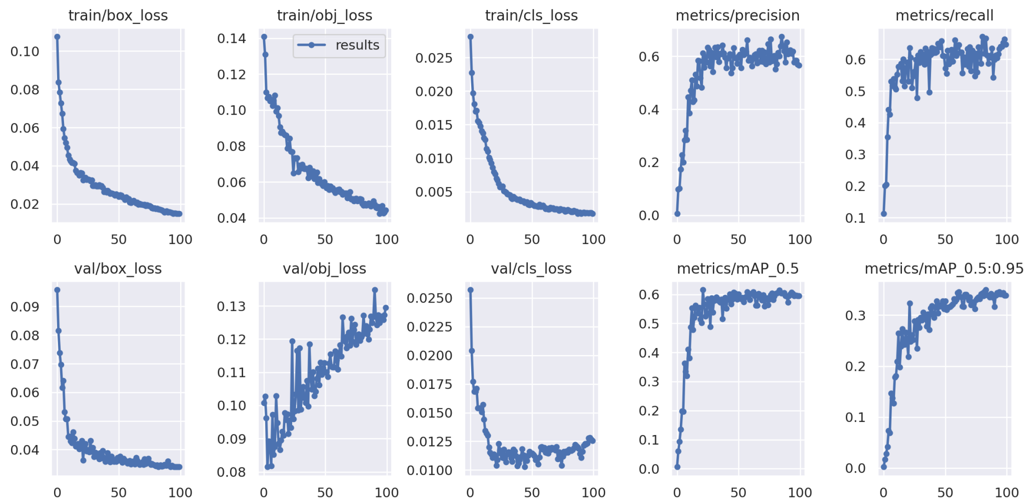

Figure 66 – Evaluation metrics (dataset of 150 images)

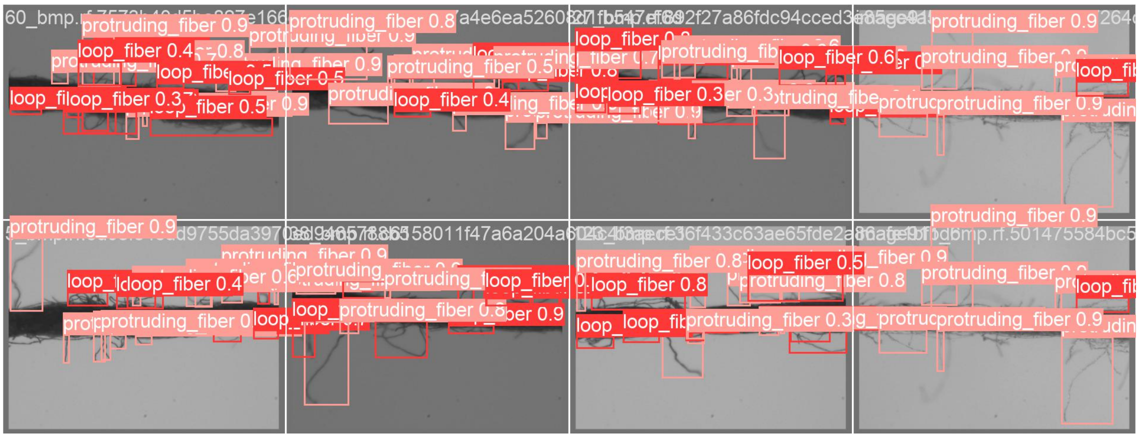

Figure 67 - Examples of classification results (dataset of 150 images)

Observing the results obtained with the dataset of 150 images, in comparison with the results of the 50 images dataset (Figure 62 and Figure 63), one can see that the overall performance improved significantly, being the approach used capable of classifying more accurately the loop and protruding fibres, as demonstrated by the confusion matrix (Figure 65) and the evaluation metrics (Figure 66). Moreover, the classification results also show that, at this phase of the study, the level of detection of hairiness and protruding fibres in the image (Figure 67), in comparison with the 50 images dataset (Figure 64), increased extremely, giving an expectation that the tested approach can give a relevant contribute to the topic.

3.3 Advantages of the Yarn Analysis and Characterization Methodologies Developed/Under Development in Comparison to Commercial Systems

This chapter presented methodologies and approaches developed or under development that offer several advantages over commercial equipment, including:

- The ability to simultaneously use coherent optical signal processing for yarn hairiness and diameter characterization [37], [40];
- Autocalibration procedures for yarn hairiness reference and diameter determination [37], [40];
- Measurement of yarn mass variation using a 1mm capacitive sensor for direct detection of nep faults [19];
- The ability to simultaneously use multiple signal processing techniques for accurate yarn periodic error characterization [36];
- Automatic determination of yarn production characteristics [8], [12];
- Development of prototypes with reduced dimensions for high portability and use in laboratory analysis or industrial yarn quality control [7],[12];
- Quantification and distinction between hairiness types (protruding/loop fibres) [9], [12].

The author is currently leading research to enhance the prototype shown in Figure 59 using computer vision algorithms for yarn quality parameterization and artificial intelligence techniques to enhance yarn characterization and improve prediction of fabric results [12], [32], [33], [56].

In summary, the techniques presented over this chapter aim to contribute to the advance of methodologies of yarn analysis and characterization in order to develop a low-cost system with superior yarn parameterization, high resolution, and precision compared to the available commercial equipment.

4 Future Challenges

Further ideas for development based on the methodologies/research undertaken or led by the author include:

- Development of custom-made photodiodes with only the necessary active area for yarn hairiness and yarn diameter determination, reducing background noise from the use of photodiodes with partially blocked active areas;
- Study of yarn hairiness spatial position based on yarn hairiness measurements using a line array of photodiodes or image processing;
- Development and further integration of an automatic yarn sample insertion system to reduce user interaction;
- Development of a method using an electric field to straighten yarn hairiness and accurately determine the length of yarn hairs using a line array or image processing;
- Determination of the experimental relationship between yarn diameter and yarn linear mass for non-100% cotton yarns;
- Development of new, optimized Fast Impulse Frequency Determination (FDFI) algorithms [36] to reduce computational effort and increase data throughput in yarn periodical errors analysis;
- Optimization of image processing algorithms for yarn parameter determination to reduce computational effort and enable real-time analysis;
- Use of artificial intelligence techniques (deep learning) to predict fabric quality based on the overall parameterization obtained from the developed/under development prototypes.

References

[1] Uster, 'Uster Tester 6', 2022. [Online]. Available: https://www.uster.com/products/staple-yarn-testing/uster-tester/

[2] Zweigle, 'Zweigle Tester´s', 2008. [Online]. Available: www.zweigle.com (retrieved on https://web.archive.org)

[3] Uster, 'Uster Zweigle', 2020. [Online]. Available: https://www.uster.com/en/instruments/staple-yarn-testing/uster-zweigle/ (retrieved on https://web.archive.org)

[4] V. Carvalho, 'Automatic Yarn Characterization System', Minho University, 2008.

[5] W. Zhang, C. Iype, and W. Oxenham, 'The analysis of yarn thin places and unevenness with an image-analysis system and program design', *The Journal of the Textile Institute*, vol. 89, no. 1, pp. 44–58, 1998, [Online]. Available: http://search.ebscohost.com/login.aspx?direct=true&db=edswsc&AN=000073164700004&site=eds-live

[6] V. Carvalho, J. G. Pinto, J. Monteiro, R. M. Vasconcelos, and F. O. Soares, 'On-line measurement of yarn evenness', in *IEEE International Symposium on Industrial Electronics*, 2003, vol. II. doi: 10.1109/ISIE.2003.1267970.

[7] V. H. Carvalho, F. O. Soares, M. S. Belsley, and R. M. Vasconcelos, 'Automatic Yarn Characterization System: Design of a Prototype', *IEEE Sens J*, vol. 9, no. 8, 2009, doi: 10.1109/JSEN.2009.2025810.

[8] V. H. Carvalho, M. S. Belsley, R. M. Vasconcelos, and F. O. Soares, 'Determination of yarn production characteristics using image processing', *Int J Imaging Syst Technol*, vol. 20, no. 4, 2010, doi: 10.1002/ima.20259.

[9] N. Gonçalves, V. Carvalho, M. Belsley, R. M. Vasconcelos, F. O. Soares, and J. Machado, 'Yarn features extraction using image processing and computer vision - A study with cotton and polyester yarns', *Measurement (Lond)*, vol. 68, 2015, doi: 10.1016/j.measurement.2015.02.010.

[10] A. Wijayono and V. G. V. Putra, 'Implementation of Digital Image Processing and Computation Technology on Measurement and Testing of Various Yarn Parameters'. 2018. [Online]. Available: http://arxiv.org/abs/1810.07649

[11] Z. Li, P. Zhong, X. Tang, Y. Chen, S. Su, and T. Zhai, 'A New Method to Evaluate Yarn Appearance Qualities Based on Machine Vision and Image Processing', *IEEE Access*, vol. 8, pp. 30928–30937, 2020, doi: 10.1109/ACCESS.2020.2972967.

[12] F. Pereira *et al.*, 'Intelligent Computer Vision System for Analysis and Characterization of Yarn Quality', *Electronics (Basel)*, vol. 12, no. 1, pp. 1–37, 2023, [Online]. Available: https://doi.org/10.3390/electronics12010236

[13] V. H. Carvalho, P. J. Cardoso, M. S. Belsley, R. M. Vasconcelos, and F. O. Soares, 'Yarn hairiness characterization using two orthogonal directions', *IEEE Trans Instrum Meas*, vol. 58, no. 3, 2009, doi: 10.1109/TIM.2008.2005082.

[14] H. R. Boswell and P. P. Townend, '11— Some Factors Affecting the Hairiness of Worsted Yarns', *Journal of the Textile Institute Transactions*, vol. 48, no. 5, pp. T135–T142, May 1957, doi: 10.1080/19447025708660075.

[15] V. Carvalho, P. Cardoso, M. Belsley, R. M. Vasconcelos, and F. O. Soares, 'Development of a yarn evenness measurement and hairiness analysis system', in *IECON Proceedings (Industrial Electronics Conference)*, 2006. doi: 10.1109/IECON.2006.347502.

[16] A. Anand, V. K. Chhaniwal, and C. S. Narayanamurthy, 'Hairiness measurement of textile yarns using crossed polarizers', *Review of Scientific Instruments*, vol. 76, pp. 76103–76104, Jul. 2005, doi: 10.1063/1.1951590.

[17] A. Barella, 'The Hairiness of Yarns', *Textile Progress*, vol. 24, no. 3, pp. 1–46, Sep. 1993, doi: 10.1080/00405169308688860.

[18] M. Günay, 'Characterization and Quantification of Woven Fabric Irregularities Using 2-D', North Carolina State, 2005.

[19] V. Carvalho, J. G. Pinto, J. L. Monteiro, R. M. Vasconcelos, and F. O. Soares, 'Yarn parameterization based on mass analysis', *Sens Actuators A Phys*, vol. 115, no. 2-3 SPEC. ISS., 2004, doi: 10.1016/j.sna.2004.04.045.

[20] N. Haleem, M. Bustreo, and A. del Bue, 'A computer vision based online quality control system for textile yarns', *Comput Ind*, vol. 133, p. 103550, 2021, doi: https://doi.org/10.1016/j.compind.2021.103550.

[21] A. El-Geiheini, S. ElKateb, and M. R. Abd-Elhamied, 'Yarn Tensile Properties Modelling Using Artificial Intelligence', *Alexandria Engineering Journal*, vol. 59, no. 6, pp. 4435–4440, 2020, doi: https://doi.org/10.1016/j.aej.2020.07.049.

[22] M. R. Abd-Elhamied, W. A. Hashima, S. ElKateb, I. Elhawary, and A. El-Geiheini, 'Prediction of Cotton Yarn's Characteristics by Image Processing and ANN', *Alexandria Engineering Journal*, vol. 61, no. 4, pp. 3335–3340, 2022, doi: https://doi.org/10.1016/j.aej.2021.08.057.

[23] L. Wang, B. Xu, and W. Gao, '3D measurement of yarn hairiness via multi-perspective images', in *Proc.SPIE*, Jul. 2018, vol. 10679, p. 1067916. doi: 10.1117/12.2307844.

[24] Y. Sun, Z. Li, R. Pan, J. Zhou, and W. Gao, 'Measurement of long yarn hair based on hairiness segmentation and hairiness tracking', *The Journal of The Textile Institute*, vol. 108, no. 7, pp. 1271–1279, Jul. 2017, doi: 10.1080/00405000.2016.1240144.

[25] J. Jing, M. Huang, P. Li, and X. Ning, 'Automatic measurement of yarn hairiness based on the improved MRMRF segmentation algorithm', *The Journal of The Textile Institute*, vol. 109, no. 6, pp. 740–749, Jun. 2018, doi: 10.1080/00405000.2017.1368106.

[26] J. Sun, J. Jia, C. K. Tang, and H. Y. Shum, 'Poisson matting', *ACM SIGGRAPH 2004 Papers, SIGGRAPH 2004*, no. 1, pp. 315–321, 2004, doi: 10.1145/1186562.1015721.

[27] P. Viola and M. Jones, 'Rapid object detection using a boosted cascade of simple features', in *Proceedings of the 2001 IEEE Computer Society Conference on Computer Vision and Pattern Recognition. CVPR 2001*, 2001, vol. 1, pp. I–I. doi: 10.1109/CVPR.2001.990517.

[28] H. Yu and B. M. Wilamowski, 'Levenberg—Marquardt Training', 2011.

[29] E. M. de M. Araújo, Mário; Castro, *Manual de Engenharia Têxtil*. Lisboa: Fundação Calouste Gulbenkian, 1986.

[30] V. Carvalho, R. M. Vasconcelos, F. O. Soares, and M. Belsley, 'Yarn diameter and linear mass correlation', *J Nondestr Eval*, vol. 28, no. 2, 2009, doi: 10.1007/s10921-009-0046-8.

[31] X.-H. Wang, J.-Y. Wang, J.-L. Zhang, H.-W. Liang, and P.-M. Kou, 'Study on the detection of yarn hairiness morphology based on image processing technique', *2010 International Conference on Machine Learning and Cybernetics, Machine Learning and Cybernetics (ICMLC), 2010 International Conference on*, vol. 5. pp. 2332–2336, 2010. doi: 10.1109/ICMLC.2010.5580660.

[32] V. Carvalho, F. Soares, and R. Vasconcelos, 'Artificial intelligence and image processing based techniques: A tool for yarns parameterization and fabrics prediction', in *ETFA 2009 - 2009 IEEE Conference on Emerging Technologies and Factory Automation*, 2009. doi: 10.1109/ETFA.2009.5347255.

[33] F. Pereira, V. Carvalho, F. Soares, R. Vasconcelos, and J. Machado, *Computer vision techniques for detecting yarn defects*. 2018. doi: 10.1016/B978-0-08-101217-8.00006-3.

[34] R. Pinto, F. Pereira, V. Carvalho, F. Soares, and R. Vasconcelos, 'Yarn linear mass determination using image processing: First insights', in *IECON Proceedings (Industrial Electronics Conference)*, 2019, vol. 2019-Octob. doi: 10.1109/IECON.2019.8926650.

[35] V. H. Carvalho, P. J. Cardoso, R. M. Vasconcelos, F. O. Soares, and M. S. Belsley, 'Optical yarn hairiness measurement system', in *IEEE International Conference on Industrial Informatics (INDIN)*, 2007, vol. 1. doi: 10.1109/INDIN.2007.4384783.

[36] V. Carvalho, M. Belsley, R. M. Vasconcelos, and F. O. Soares, 'Yarn periodical errors determination using three signal processing approaches', *Digital Signal Processing: A Review Journal*, vol. 23, no. 5, 2013, doi: 10.1016/j.dsp.2013.06.003.

[37] V. Carvalho, P. Cardoso, M. Belsley, R. M. Vasconcelos, and F. O. Soares, 'Yarn hairiness parameterization using a coherent signal processing technique', *Sens Actuators A Phys*, vol. 142, no. 1, 2008, doi: 10.1016/j.sna.2007.02.019.

[38] R. M. Sillitto, 'The Fourier Transform and Its Applications to Optics', *Optica Acta: International Journal of Optics*, vol. 31, no. 1, p. 2, Jan. 1984, doi: 10.1080/713821392.

[39] J. H. Madsen, Christi;Zhao, 'Optical Measurements and Filter Analysis', in *Optical Filter Design and Analysis*, 1999, pp. 355–395. doi: 10.1002/0471213756.ch7.

[40] V. H. Carvalho, P. J. Cardoso, M. S. Belsley, R. M. Vasconcelos, and F. O. Soares, 'Yarn diameter measurements using coherent optical signal processing', *IEEE Sens J*, vol. 8, no. 11, 2008, doi: 10.1109/JSEN.2008.2005231.

[41] V. Carvalho, F. Soares, R. Vasconcelos, M. Belsley, and N. Gonçalves, 'Yarn hairiness determination using image processing techniques', in *IEEE International Conference on Emerging Technologies and Factory Automation, ETFA*, 2011. doi: 10.1109/ETFA.2011.6059217.

[42] N. Goncalves, V. Carvalho, F. Soares, and R. Vasconcelos, 'Studies on the yarn mass parameters determination using Image Processing techniques', in *IEEE International Conference on Emerging Technologies and Factory Automation, ETFA*, 2012. doi: 10.1109/ETFA.2012.6489765.

[43] V. Carvalho, N. Gonçalves, F. Soares, R. Vasconcelos, and M. Belsley, 'Yarn parameterization and fabrics prediction using image processing'. 2013. [Online]. Available: http://hdl.handle.net/1822/27424

[44] J. G. Pinto, J. Monteiro, R. Vasconcelos, and F. O. Soares, 'A new system for direct measurement of yarn mass with 1mm accuracy', *Proceedings of the IEEE International Conference on Industrial Technology*, vol. 2, pp. 1158–1163, 2002, doi: 10.1109/ICIT.2002.1189336.

[45] V. Carvalho, P. Cardoso, M. Belsley, and R. M. Vasconcelos, 'A New Statistical Reference Method for Yarn Hairiness Quantification', in *IEEE International Symposium on Industrial Electronics*, 2007, pp. 1–7.

[46] V. Carvalho, F. O. Soares, R. M. Vasconcelos, and M. Belsley, 'A comparative study between yarn diameter and yarn mass variation measurement systems using capacitive and optical sensors', *Indian J Fibre Text Res*, vol. 33, no. 2, 2008.

[47] S. Franco, *Design with Operational Amplifiers and Analog Circuits*, 4th ed. New York: McGraw-Hill Education OP - AccessScience, 2002.

[48] A. Sparavigna, E. Broglia, and S. Lugli, 'Beyond capacitive systems with optical measurements for yarn evenness evaluation', *Mechatronics*, vol. 14, no. 10, pp. 1183–1196, 2004, doi: https://doi.org/10.1016/j.mechatronics.2004.07.002.

[49] P. Caldas, F. Sousa, F. Pereira, H. Lopes, and J. Machado, 'Automatic system for yarn quality analysis by image processing', *Journal of the Brazilian Society of Mechanical Sciences and Engineering*, vol. 44, no. 11, p. 565, 2022, doi: 10.1007/s40430-022-03875-3.

[50] Roboflow, 'Roboflow'. https://roboflow.com (accessed Jan. 14, 2023).

[51] MIT, 'LabelME'. http://labelme2.csail.mit.edu/ (accessed Jan. 13, 2023).

[52] M. Horvat, L. Jelecevic, and G. Gledec, 'A comparative study of YOLOv5 models performance for image localization and classification', in *Proceedings of the 33rd Central European Conference on Information and Intelligent Systems (CECIIS)*, 2022, pp. 349–356.

[53] J. Redmon, S. Divvala, R. Girshick, and A. Farhadi, 'You Only Look Once: Unified, Real-Time Object Detection', in *2016 IEEE Conference on Computer Vision and Pattern Recognition (CVPR)*, 2016, pp. 779–788. doi: 10.1109/CVPR.2016.91.

[54] H. Dalianis, 'Evaluation Metrics and Evaluation', in *Clinical Text Mining*, no. 1967, 2018, pp. 45–53. doi: 10.1007/978-3-319-78503-5_6.

[55] H. Rezatofighi, N. Tsoi, J. Gwak, A. Sadeghian, I. Reid, and S. Savarese, 'Generalized intersection over union: A metric and a loss for bounding box regression', *Proceedings of the IEEE Computer Society Conference on Computer Vision and Pattern Recognition*, vol. 2019-June, pp. 658–666, 2019, doi: 10.1109/CVPR.2019.00075.

[56] F. Pereira, V. Carvalho, R. Vasconcelos, and F. Soares, 'A review in the use of artificial intelligence in textile industry', in *Lecture Notes in Mechanical Engineering*, 2020, pp. 1–12.